Laterally Transported Particles From Margins Serve as a Major Carbon and Energy Source for Dark Ocean Ecosystems

Jiaming Shen[1] ![ID], Nianzhi Jiao[1] ![ID], Minhan Dai[1] ![ID], Haili Wang[1] ![ID], Guoqiang Qiu[1] ![ID], Jianfang Chen[2] ![ID], Hongliang Li[2], Shuh-Ji Kao[1] ![ID], Jin-Yu Terence Yang[1] ![ID], Pinghe Cai[1], Kuanbo Zhou[1], Weifeng Yang[1] ![ID], Yifan Zhu[1], Zhiyu Liu[1] ![ID], Mingming Chen[1], Zuhui Zuo[1], Birgit Gaye[3], Martin G. Wiesner[2,3], and Yao Zhang[1] ![ID]

[1]State Key Laboratory of Marine Environmental Sciences and College of Ocean and Earth Sciences, Xiamen University, Xiamen, China, [2]Key Laboratory of Marine Ecosystem and Biogeochemistry, Second Institute of Oceanography, State Oceanic Administration, Hangzhou, China, [3]Institute of Geology, University of Hamburg, Hamburg, Germany

Abstract Deep ocean microorganisms consume particulate organic matter that is produced in the surface ocean and exported to deeper depths. Such consumption not only enriches inorganic carbon in the deep ocean but also transforms organic carbon into recalcitrant forms, creating an alternative type of carbon sequestration. However, estimates of deep microbial carbon demand substantially exceed the available particulate organic carbon exported from the euphotic zone, resulting in an unbalanced dark ocean carbon budget. Here, we combined field-based microbial activity parameters, integrated multiyear particle export flux data, sinking particle fluxes measured by sediment traps, and optical data from Biogeochemical-Argo floats to quantify the main sources of organic carbon to the dark ocean. Laterally transported particles (including sinking and suspended particles) serve as a major energy source, which directly provide organic carbon and enhance new organic carbon production by dark carbon fixation, reconciling the mismatch in the regional carbon budget.

Plain Language Summary Particulate organic matter, produced by phytoplankton in the upper ocean, can sink through the water column and act as a source of organic matter to the deep ocean. These particles are decomposed to carbon dioxide by microorganisms, resulting in dissolved inorganic carbon and organic carbon resistant to decomposition in the deeper ocean. This process controls the biological sequestration of CO_2 by the oceans. However, there is an imbalance between the low amount of organic carbon exported from the photic zone and the high microbial demand for carbon in the dark ocean. We attempted to explain how the deep ocean carbon and energy supply can meet the microbial metabolic demand. Four main organic carbon sources were measured and quantified in the South China Sea: particles that come from the photic zone, particles that move laterally through the ocean, dark carbon fixation, and dissolved organic carbon. We found that laterally transported particles from the surrounding margins provide a direct source of organic carbon and also allow for much new organic carbon production through dark carbon fixation. These particles, which provide a major energy source to dark ocean ecosystems, help resolve the mismatch in the regional carbon budget.

1. Introduction

The dark ocean (i.e., below the photic zone) accounts for ~70% of the global ocean volume and represents one of the largest biomes on Earth (Galand et al., 2009). This realm is characterized by low temperature and high hydrostatic pressure, and most of the dissolved organic carbon (DOC) is present as recalcitrant DOC (RDOC; Arístegui et al., 2009). These conditions seem to inhibit the metabolic capacity of living organisms, but a growing amount of data indicates that the dark ocean contains diverse and active microbial communities (Baltar, Arístegui, Gasol, Sintes, et al., 2010; Teira et al., 2006; Zhang, Zhao, et al., 2014). These microorganisms utilize particulate organic matter (POM) sourced from the euphotic zone for respiration to enrich dissolved inorganic carbon (DIC) for storage in the deep ocean, constituting the final step of the biological pump (Herndl & Reinthaler, 2013). Additionally, these microorganisms transform labile POM into RDOC that allows for a much longer turnover of stored carbon, known as the microbial carbon pump (Jiao et al., 2010). Therefore, microbial activity at depth essentially controls carbon sequestration by the ocean.

Sinking POM from the euphotic zone has been thought to provide the most important carbon and energy source to the dark ocean (Nagata et al., 2000; Suess, 1980). However, studies in the Atlantic Ocean found that the carbon demand of heterotrophic microbes is one to two magnitudes higher than the input of sinking particles (Herndl & Reinthaler, 2013; Reinthaler et al., 2006), which results in a substantial imbalance in the carbon budget of the dark ocean. To date, it is not known how the deep ocean carbon supply meets microbial metabolic demand. Two extra carbon sources could partly alleviate this mismatch. The first is suspended (slow-sinking and buoyant) particles that are largely underestimated in sediment trap data and difficult to determine directly (Baltar et al., 2009; Baltar, Arístegui, Sintes, et al., 2010), and the second is DIC fixation by chemolithoautotrophic archaea and bacteria in the deep ocean (Herndl et al., 2005; Zhang et al., 2020).

There is an unconstrained carbon/energy source supplying microbial carbon demand at depth. Laterally transported particles from the continental margin to the deep open ocean by hyperpycnal flows, eddies, and lateral diffusion and intrusion (Gao et al., 2015; Hwang et al., 2008) could provide significant energy to the dark ocean ecosystems (Burd et al., 2010; Nakatsuka et al., 2004). One model estimated that laterally transported particulate flux accounted for 28–59% of the total mesopelagic respiration in the Canary Current region of the subtropical northeastern Atlantic Ocean (Alonso-González et al., 2009). Despite the importance of laterally transported particles, we still lack direct observations to test whether this source of carbon balances the deep ocean carbon budget, as well as a quantitative, mechanistic understanding of key parts of the dark ocean carbon budget.

The South China Sea (SCS; Figure 1a), located in the (sub)tropical western North Pacific Ocean, is one of the world's largest marginal seas (Geng et al., 2019). Although it receives input from the Pearl and Gaoping Rivers in the north and the Mekong River in the south, the SCS is an oligotrophic ocean-dominated marginal sea with a deep basin and a permanently stratified central gyre (Dai et al., 2013; Gong et al., 1992). Basin-scale upper-layer circulation is driven by the East Asian monsoon and the Kuroshio Current, a North Pacific subtropical western boundary surface current (Wang et al., 2003). Mesopelagic and bathypelagic waters are transported westward into the SCS from the western Pacific through the Luzon Strait (Liu & Liu, 1988) and turn northwestward and then southwestward along the continental margin as a contour current (Qu et al., 2006). These ocean currents generally constrain the exchange between the coastal and open ocean waters. However, strong middeep mixing of the SCS could promote distinctly lateral transports (Wang et al., 2019). Therefore, the SCS is an ideal environment to determine the contribution of laterally transported particles to the dark ocean ecosystem.

We performed a comprehensive analysis of organic carbon supply and microbial demand in the deep SCS, combining bacterial biomass production, dark carbon fixation, and nitrifier abundance measurements with integrated multiyear particle export flux measurements, sinking particle fluxes measured by sediment traps, ammonium and nitrite concentrations, and optical-based particle and fluorescent dissolved organic matter (FDOM) concentrations collected by Biogeochemical-Argo (BGC-Argo) floats. Finally, we estimated the contributions of the main carbon/energy sources to the dark ocean carbon demand: exported particles, laterally transported particles, dark carbon fixation, and DOC. We found distinct differences in these contributions between the northern SCS (NSCS; 17–22°N) and the southern SCS (SSCS; 10–17°N).

2. Methods

The study area covered the entire SCS (water depth > 200 m) over six survey cruises from 2014 to 2018 (Figure 1a). Seawater was collected throughout the water column for measurements of bacterial production (BP), leucine-to-carbon conversion factors, microbial DIC fixation rates, and gene abundances of size-fractional ammonia-oxidizing archaea (AOA) *amo*A and nitrite-oxidizing bacteria (NOB) *Nitrospina* 16S rRNA. Bacterial carbon demand (BCD) was estimated using Equation 1 (Del Giorgio & Cole, 1998):

$$BCD = \frac{BP}{BGE}, \tag{1}$$

where *BGE* is the bacterial growth efficiency. We collated all published BGE values below 100 m from the Pacific, Atlantic, and Indian Oceans, which were estimated from bacterial respiration rates calculated from dissolved oxygen concentrations (Baltar, Arístegui, Gasol, & Herndl, 2010; Biddanda et al., 1997; Mazuecos et al., 2015; Motegi et al., 2009; Reinthaler et al., 2006; Uchimiya et al., 2015; supporting
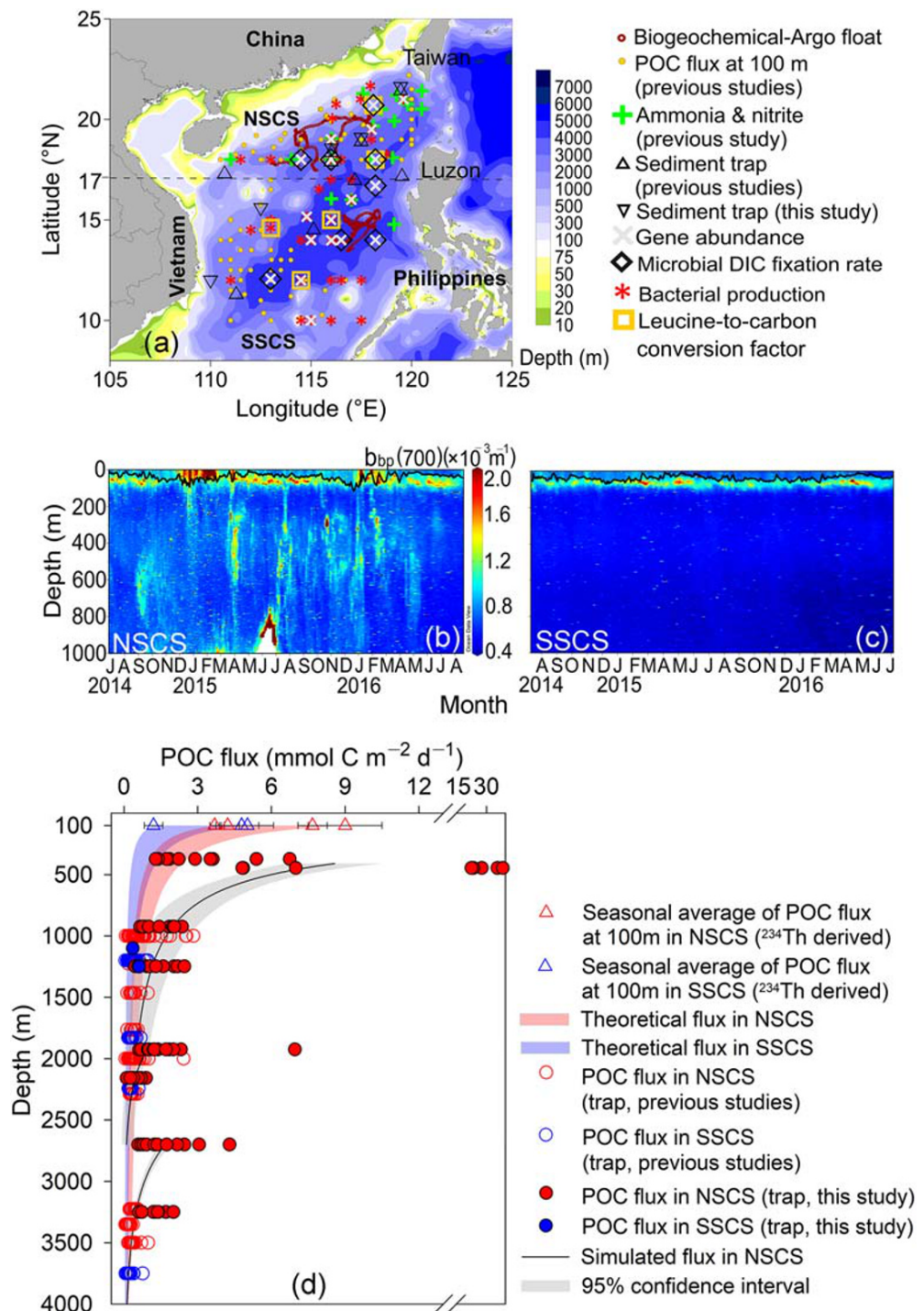
Figure 1. (a) Sampling sites in the South China Sea (SCS). Isobaths on the map are used as the background, and the color bar indicates water depth. Particulate backscattering coefficient at 700 nm ($b_{bp}(700)$) collected from Biogeochemical-Argo floats in the (b) northern SCS (NSCS) basin and (c) southern SCS (SSCS) basin. Black lines represent the mixed-layer depth. (d) Vertical distribution of sinking particulate organic carbon (POC) flux (reference data were combined; see Tables S1 and S2). The seasonal averages (error bars represent standard error) of export flux at 100 m in the NSCS and SSCS are shown. Theoretical fluxes (red and blue) below 100 m were simulated by the Martin curve. The sinking fluxes (black lines) of POC measured by sediment traps were also fitted by the Martin curve (411–1,924, 1,925–2,699, and 2,700–4,000 m; $p < 0.01$). The gray areas show 95% confidence intervals.

information Figure S1). The mean values of these three oceans (7%) and the Pacific Ocean individually (3%) were used to estimate BCD.

Two SeaBird Navis-BGCi floats, equipped with an SBE 41CP conductivity-temperature-depth profiler, an SBE 63 dissolved oxygen sensor, and a WET Labs ECO-MCOMS optical sensor, were deployed in the NSCS (float serial number "0347") on 26 June 2014 and in the SSCS ("0348") on 10 July 2014 to acquire a 2-year time-series data set. Their trajectories are shown in Figure 1a. Particulate backscattering coefficient at 700 nm ($b_{bp}(700)$), fluorescence of FDOM, apparent oxygen utilization, temperature, and salinity were used in this study.

Data on thorium-derived particulate organic carbon (POC) export at 100 m were collected from previous studies (Cai et al., 2008, 2015; Jiao et al., 2014; Yang et al., 2015; Zhou et al., 2013; Table S1). Theoretical POC and particulate nitrogen (PN) flux values below 100 m were estimated based on a Martin curve (Martin et al., 1987) using a power law Equation 2:

$$F_z = F_{Z_0} \left(\frac{Z}{Z_0} \right)^{-b}, \tag{2}$$

where F_z is the flux at depth z, normalized to flux at some reference depth z_0, and b is the coefficient of flux attenuation. The b value was estimated as 0.95 for POC and 1.02 for PN using the average flux at 100 m and the sinking flux of POC measured by sediment traps in the SSCS where lateral transport of particles was not observed (Figure 1c).

Particles were collected to estimate sinking POC flux from a combination of lateral and vertical processes using bottom-anchored time-series sediment traps (McLane Mark 7G-21 and Technicap PPS 3/3) deployed at 374–3250 m (one to four depth layers) at three stations in the NSCS and two in the SSCS (Table S2). Additional trap data (367 values for POC and 350 values for PN) from previous studies were also used (Gaye et al., 2009; Kao et al., 2012; Lahajnar et al., 2007; Ran et al., 2015; Tan et al., 2020; Wei et al., 2017; Zhang et al., 2019; Table S2). These trap fluxes were also fitted to a Martin curve using Equation 2. The sinking fluxes of laterally transported POC and PN (F_{LTS}) were estimated using Equation 3:

$$F_{LTS} = \sum_{n=1}^{n-1} \left(F_{TrapMC_n(Max)} - F_{TrapMC_n(Min)} \right) + F_{TrapMC_n(Max)} - F_{(Z_1)}, \tag{3}$$

where n represents the number of episodic pulses of laterally transported particles at different depths into the deep sea, $F_{TrapMC_n(Max)}$ and $F_{TrapMC_n(Min)}$ are the flux maximum and minimum, respectively, on the Martin curve, and $F_{(Z_1)}$ is the theoretical flux calculated from Equation 2 at the depth of the first lateral pulse (Figure 1d). Other detailed descriptions are provided in the supporting information.

3. Results and Discussion

3.1. POC Flux and Lateral Particle Transport

The NSCS seasonally averaged POC flux at 100-m depth was 7.7 $\pm$ 0.6 (standard error or propagated error; $n = 21$) mmol C m^{-2} day^{-1} in spring, 3.7 $\pm$ 0.2 ($n = 41$) mmol C m^{-2} day^{-1} in summer, 9.0 $\pm$ 1.5 ($n = 11$) mmol C m^{-2} day^{-1} in autumn, and 4.2 $\pm$ 0.5 ($n = 17$) mmol C m^{-2} day^{-1} in winter (Table S1). The SSCS seasonally averaged POC flux at 100 m was 5.0 $\pm$ 1.1 ($n = 13$), 4.8 $\pm$ 0.7 ($n = 23$), and 1.2 $\pm$ 0.4 ($n = 7$) mmol C m^{-2} day^{-1} in spring, summer, and autumn, respectively. There were few clear seasonal differences in POC flux; this homogeneity was especially clear in the SSCS because it is the low-latitude high-sunlight region. The only significant differences in POC flux at 100 m were found in spring (Mann-Whitney U test; $p < 0.05$) and autumn ($p < 0.01$) between the NSCS and SSCS. Therefore, higher theoretical fluxes, based on the Martin curve, below 100 m were observed in the NSCS than the SSCS. Consistently, the sinking fluxes of POC and PN throughout mesopelagic and bathypelagic waters, estimated by sediment traps, were also higher in the NSCS than SSCS ($p < 0.01$; Figures 1d and S2). Notably, the sediment trap-based estimated fluxes were mostly higher than the theoretical fluxes in the NSCS (up to ~30× higher). Episodic fluxes were mainly observed at 374–447 m (average depth 411 m, 10.2 $\pm$ 2.7 mmol C m^{-2} day^{-1}), 1,925 m (1.8 $\pm$ 0.5 mmol C m^{-2} day^{-1}), and 2,700 m

$(1.7 \pm 0.3 \text{ mmol C m}^{-2} \text{ day}^{-1})$; trap-based sinking fluxes were statistically fitted by a Martin curve into three zones split by three depths (411, 1,925, and 2,700 m; Figure 1d). Moored traps, such as those used in this study, can suffer from advection perturbations, causing particles to be overcollected or undercollected (Buesseler et al., 2007); however, an analysis of integrated multiyear data from all stations covering the entire SCS reduces this uncertainty.

The wide gap between the theoretical and observed fluxes in the NSCS suggests that a large portion of the sinking particles collected by sediment traps could have been laterally transported from the surrounding margins. We estimated that $60 \pm 11\%$ of the sinking POC of the NSCS is derived from laterally transported particles based on the difference between the export flux at 100 m and simulated curves of trap fluxes below 100 m; this estimate rose to $85 \pm 14\%$ below 374 m where lateral transport starts to be considered. The estimates of laterally transported POC were similar to those estimated via the PN flux ($50 \pm 12\%$ and $81 \pm 16\%$ below 100 and 374 m, respectively, in this study; 45–80% in intermediate and deep waters in Yang et al., 2017). The strong lateral transport in the SCS has been demonstrated by detrital clay composition, particle morphology and composition, and $\delta^{15}N$ in sinking particles (Schroeder et al., 2015; Shih et al., 2019; Yang et al., 2017). BGC-Argo floats provide direct evidence of episodic pulses of particles into the deep sea, and based on 2 years of in situ observations, these pulses occurred almost monthly between the continental shelf and the deep basin (Figure 1b). In contrast, the particles were attenuated sharply below the euphotic zone in the SSCS (Figures 1c and S3). In general, transport from ocean margins to the open ocean are dynamically prohibited because oceanic currents tend to flow along constant depth contours (i.e., contour currents; Spall & Pedlosky, 2018). Nevertheless, transport in the SCS can be facilitated by wind forcing, eddies (Xiu et al., 2010; Zhang, Liu, et al., 2014), dense water cascades, and hyperpycnal flows (Kao et al., 2010), as well as bottom boundary layer processes (Schroeder et al., 2015). For instance, numerous energetic mesoscale eddies generated in the NSCS each year penetrate into the deep-sea and transport sediments into deep water when propagating along the slope (Zhang, Liu, et al., 2014); a typhoon in 2009 triggered storm-induced hyperpycnal flows from the Gaoping River (Taiwan), which entrained suspended sediments and directly transported them to the deep sea (Kao et al., 2010). Water mass characteristics of NSCS versus SSCS and the distribution of particles among water masses also reflected potential lateral transport in the NSCS (Figure S4). Apparently, the laterally transported particles supply a significant carbon and energy source to the deep areas of the SCS.

3.2. Reduced Nitrogen, Nitrifiers, and Dark Carbon Fixation

Significantly higher ammonium concentrations were measured below 200 m in the NSCS (0.9–44.4 nM) compared with the SSCS (0.7–20.7 nM; $p < 0.01$; Figure 2a; Zhu, 2015), corresponding to the higher POC export, strong lateral transport, and resulting higher particle concentrations. This is attributed to the remineralization of particles, since dissolved organic nitrogen exists in a refractory form in the deep ocean (Broek et al., 2019). Unlike ammonium, nitrite concentrations were equally low in the NSCS and SSCS below 200 m (Figure 2b; Zhu, 2015). Ammonia oxidation is almost the exclusive source of nitrite in oxygen-rich deep water, and nitrite is subsequently rapidly oxidized to nitrate. In the two steps of oxidations, ammonia oxidation has been verified as the rate-limiting step (Zhang et al., 2020). Therefore, higher abundances of AOA were observed in both particle-associated (>3 μm; below 200 m) and free-living communities (0.22–3 μm; below 1,000 m) in the NSCS compared with the SSCS ($p < 0.01$; Figures 2c and 2d), corresponding to the higher ammonium concentration in the NSCS. Particle-associated NOB *Nitrospina* abundances were also higher below 200 m in the NSCS than in the SSCS ($p < 0.05$–0.01; Figures 2e and 2f and Text S2).

AOA- and NOB-mediated nitrification sustains dark carbon fixation, which provides new organic matter to heterotrophic food webs in the deep ocean (Wuchter et al., 2006). The DIC fixation rate showed an exponential decrease with depth from 100 m, ranging from 20.25 to 0.15 μmol C m^{-3} day^{-1} in the NSCS and 11.10 to 0.01 μmol C m^{-3} day^{-1} in the SSCS. Significantly higher DIC fixation rates were observed below 200 m in the NSCS than those in the SSCS ($p < 0.05$–0.01; Figure 2g), which was consistent with higher ammonium concentrations and particle-associated nitrifier abundances in the NSCS. The integrated DIC fixation between 100 and 4,000 m was 2.4× higher in the NSCS than the SSCS. The degree of difference between the NSCS and SSCS in DIC fixation (2.4) was higher than the export flux at 100 m between the two basins (NSCS was 1.7-fold higher than SSCS), so there must be additional energy sources beyond reduced nitrogen from exported POM remineralization to support high DIC fixation rates in the deep
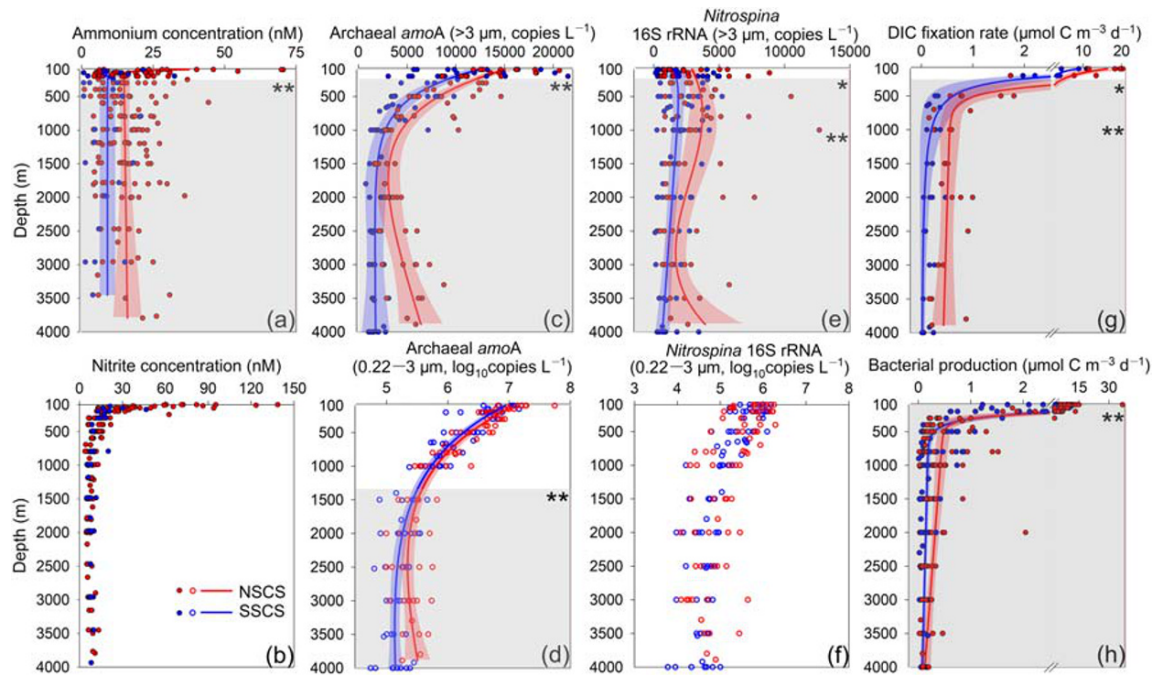
Figure 2. Depth profiles of (a) ammonium and (b) nitrite concentrations (data from Zhu, 2015), (c, e) particle-associated (>3 μm), and (d, f) free-living (0.22–3 μm) archaeal *amo*A (in c and d) and *Nitrospina* 16S rRNA (in e and f) gene abundances, (g) dissolved inorganic carbon (DIC) fixation rates, and (h) bacterial production. The red (northern South China Sea; NSCS) and blue (southern South China Sea; SSCS) lines are the fitted curves ($p < 0.05$–0.01). The shaded areas show 95% confidence intervals. The gray background indicates a significant difference (Mann-Whitney U test) for a given depth zone between the NSCS and SSCS. [*]$p < 0.05$; [**]$p < 0.01$.

NSCS. The degree of difference in DIC fixation was lower than the difference in trap flux attenuation where the NSCS was 3.4-fold higher than the SSCS. This suggests that laterally transported particles can supply extra energy to stimulate dark carbon fixation in the NSCS. In addition to reduced nitrogen, POM has been reported to provide reduced sulfur compounds, urea, and iron to facilitate chemoautotrophic production (Hsiao et al., 2014; Kitzinger et al., 2018; Swan et al., 2011). Besides nitrifiers, other microbial groups, such as SAR324 (Deltaproteobacteria), SAR406 (Marinimicrobia), SAR202 (Chloroflexi), and *Alteromonas* (Gammaproteobacteria), have demonstrated through microautoradiography combined with catalyzed reported deposition-fluorescence in situ hybridization to be capable of DIC fixation (Guerrero-Feijóo et al., 2018). Heterotrophs were found to incorporate CO_2 via anaplerotic metabolism, which would be enhanced as the availability of organic carbon increased (Baltar et al., 2016; Erb, 2011). Therefore, a higher particle flux could promote DIC fixation and supply new organic carbon to meet microbial demand.

3.3. Microbial Heterotrophic Activity and Carbon Demand

High organic carbon supply could also stimulate high microbial heterotrophic activity. The carbon conversion factor of microbial leucine incorporation was 0.37–0.55 kg C mol Leu^{-1} in the NSCS and 0.29–0.43 kg C mol Leu^{-1} in the SSCS (Figure S5). These values were comparable to those previously reported in the Pacific and Atlantic Oceans (Alonso-Sáez et al., 2007; Del Giorgio et al., 2011; Gasol et al., 2009; Morán et al., 2004; Sherr et al., 1999; Vázquez-Domínguez et al., 2008; Zubkov et al., 2000; Table S3). There were no differences across water depths. Therefore, the two average values were used to convert leucine incorporation into BP in the NSCS (0.47 kg C mol Leu^{-1}) and SSCS (0.34 kg C mol Leu^{-1}). Notably, BP was within the same order of magnitude as DIC fixation at each depth, ranging from 0.02 to 36.79 μmol C m^{-3} day^{-1} in the NSCS and 0.01 to 11.89 μmol C m^{-3} day^{-1} in the SSCS. Significantly higher BP was also observed below 100 m in the NSCS than in the SSCS ($p < 0.01$; Figure 2h).

The estimated BCD, based on BP and BGE (7% or 3%; see section 2), showed a similar depth pattern as the BP (Figures 3a and 3b). There was also a significant difference in BCD below 100 m between the NSCS and SSCS
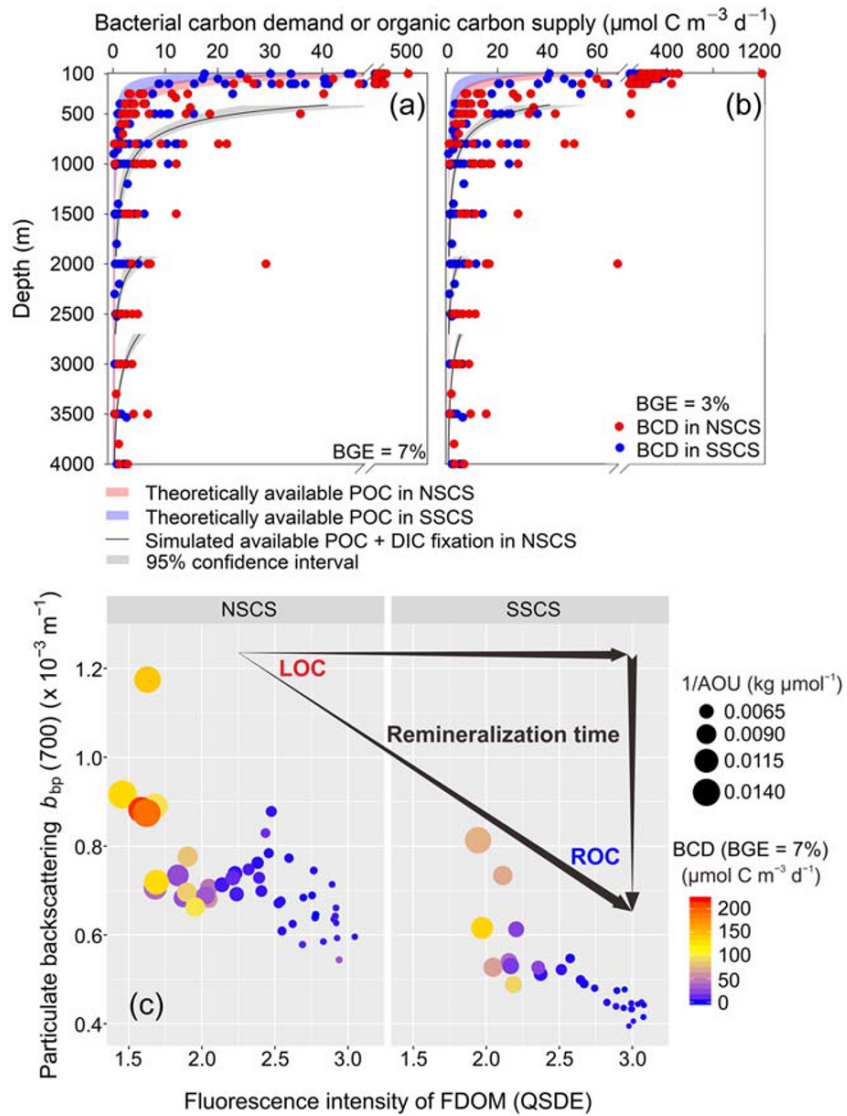
Figure 3. The estimated bacterial carbon demand (BCD) based on bacterial production and bacterial growth efficiency (BGE) of (a) 7% and (b) 3%. The theoretically available particulate organic carbon (POC; shown in red and blue) and simulated available POC (black lines) were estimated based on the theoretical flux and sinking particle flux in Figure 1, respectively (using a differential equation dF/dz, where F is flux and z is depth). For the latter, dissolved inorganic carbon (DIC) fixation was added to the output of the flux model at 411, 1,925, and 2,700 m. The gray areas show 95% confidence intervals. (c) Relationships among BCD, particulate backscattering coefficients, intensity of fluorescent dissolved organic matter (FDOM), and apparent oxygen utilization (AOU; spearman, $p < 0.05$–0.01 for each pair). The conceptual diagram in the top right corner of (c) showing decreasing POC and increasing FDOM with remineralization time suggests labile organic carbon (LOC) degradation and recalcitrant organic carbon (ROC) accumulation in the ocean's interior with particle remineralization.

($p < 0.01$). As expected, the BCD was mostly higher than the theoretical fluxes in the whole SCS and up to 2 orders of magnitude higher in both NSCS and SSCS bathypelagic zones. The depth-integrated BCD between 100 and 4,000 m was 31.4 ± 2.2 (BGE 7%) to 73.3 ± 5.1 (3%) mmol C m^{-2} day^{-1} in the NSCS and 16.2 ± 0.8 (7%) to 37.8 ± 1.9 (3%) mmol C m^{-2} day^{-1} in the SSCS. Therefore, there was a greater imbalance in the carbon budget of the deep NSCS between POC exported from 100 m and the BCD compared with the SSCS (Table 1). Microbial respiration was not measured in this study, but these values would likely add some uncertainties in the calculated BCD.

Table 1
Supply of Organic Carbon and Contributions to Total Bacterial Carbon Demand (BCD) at 100–4,000 m Depth

| Area | Depth (m) | Supply of organic carbon (mmol C m^{-2} day^{-1}) | | | Integrated BCD (mmol C m^{-2} day^{-1}) | Contribution to BCD (%) | | | |
		POC exported from 100 m[a]	Laterally transported sinking POC	Integrated DIC fixation		POC exported from 100 m	Laterally transported sinking POC	Integrated DIC fixation	Total
NSCS	100–4,000	5.9 ± 1.7	9.0 ± 1.2	4.1 ± 0.5	31.4 ± 2.2 (7%)[b]	18.8 ± 5.6	28.8 ± 4.2	13.1 ± 1.8	60.7 ± 8.0
					73.3 ± 5.1 (3%)	8.1 ± 2.4	12.3 ± 1.8	5.6 ± 0.8	26.0 ± 3.4
	100–1,000	5.4 ± 1.7	5.9 ± 1.2	2.6 ± 0.4	18.9 ± 1.5 (7%)	28.7 ± 9.3	31.4 ± 7.0	13.8 ± 2.4	73.8 ± 12.8
					44.0 ± 3.4 (3%)	12.3 ± 4.0	13.5 ± 3.0	5.9 ± 1.0	31.7 ± 5.5
	1,000–4,000	0.5 ± 0.2	3.1 ± 0.7	1.4 ± 0.2	12.6 ± 1.6 (7%)	4.0 ± 1.6	24.6 ± 6.1	11.1 ± 2.1	39.7 ± 7.6
					29.3 ± 3.8 (3%)	1.7 ± 0.7	10.6 ± 2.7	4.8 ± 0.9	17.1 ± 3.3
SSCS	100–4,000	3.6 ± 1.4	nd	1.7 ± 0.1	16.2 ± 0.8 (7%)	22.2 ± 8.7	nd	10.5 ± 0.8	32.6 ± 8.8
					37.8 ± 1.9 (3%)	9.5 ± 3.7		4.5 ± 0.3	14.0 ± 3.8
	100–1,000	3.3 ± 1.4	nd	1.2 ± 0.1	11.9 ± 0.7 (7%)	27.6 ± 11.9	nd	10.1 ± 1.0	37.7 ± 12.1
					27.7 ± 1.7 (3%)	11.9 ± 5.1		4.3 ± 0.4	16.2 ± 5.2
	1,000–4,000	0.3 ± 0.2	nd	0.5 ± 0.1	4.4 ± 0.3 (7%)	6.9 ± 3.7	nd	11.4 ± 2.4	18.3 ± 4.5
					10.2 ± 0.8 (3%)	3.0 ± 1.6		4.9 ± 1.1	7.9 ± 2.0

Note. The associated error is the standard error. nd = no data.
[a]Estimates based on the mean of seasonally averaged particulate organic carbon (POC) fluxes at 100 m.   [b]The 7% and 3% in brackets represent the bacterial growth efficiency (BGE) values used in estimating BCD.

3.4. Contributions of Various Carbon Sources to the BCD of the Dark Ocean

The attenuation of POC flux represents the POC that is theoretically consumed by deep-dwelling microbes. The POC exported from 100 m supplied 5.9 ± 1.7 and 3.6 ± 1.4 mmol C m^{-2} day^{-1} in the NSCS and SSCS, respectively, to the deep ocean (100–4,000 m) and contributed 8–22% of the total BCD (Table 1). The difference between the sinking flux of POC measured in sediment traps and the theoretical flux represents laterally derived sinking POC; this was estimated to supply 9.0 ± 1.2 mmol C m^{-2} day^{-1} to the deep NSCS, according to the attenuation of the simulated curves in three zones (Figure 1d), and contributed 12–29% of the total BCD (Table 1). The depth-integrated dark DIC fixation was 4.1 ± 0.5 and 1.7 ± 0.1 mmol C m^{-2} day^{-1} in the NSCS and SSCS, respectively, which accounts for 5–13% of the total BCD. Notably, laterally transported POC was the largest carbon source in the NSCS, accounting for 47% in the water below 100 m and 62% in the bathypelagic zone (1,000–4,000 m).

While a greater imbalance in the carbon budget between POC export and BCD at depth was present in the NSCS, laterally transported particles supply a substantial proportion of the NSCS BCD. Particularly in the bathypelagic zone, laterally transported particles contribute an order of magnitude higher amount of organic carbon to the BCD (up to ~25%) than exported POC. This reconciles a larger part of the imbalance in the carbon budget compared to previous studies of the North Atlantic Ocean where a >90% gap remains (Herndl & Reinthaler, 2013; Reinthaler et al., 2006). In the mesopelagic zone (100–1,000 m), laterally transported sinking particles result in an almost balanced organic carbon supply (up to ~74% of BCD) and demand in the NSCS, while a 70–90% gap remains in the subtropical North Pacific (Steinberg et al., 2008). In our assessment, an accurate temporal (un)coupling between organic carbon supply and BCD was not considered, but this might add some uncertainties to the carbon budget (Uchimiya et al., 2018). It could be difficult to extrapolate the estimated contributions of laterally transported particles in the SCS to a global scale.

Moreover, in our estimation, laterally transported POC has been underestimated because suspended small (nonsinking) particles are missed by sediment traps. This portion may be important to reconcile the mismatch in the carbon budget (Baltar et al., 2009; Herndl & Reinthaler, 2013). The BGC-Argo optical sensors measured backscattering of both sinking and suspended particles in the ocean (Briggs et al., 2020). Significantly positive correlations were observed between BCD and the particle backscattering coefficient (Spearman, $p < 0.05$–0.01; Figure 3c), suggesting that particles (including both sinking and suspended) serve as labile carbon and energy sources for microbial metabolism in the dark ocean. This finding is consistent with previous studies in the Atlantic where relationships were found between suspended POC and respiration rates (Baltar et al., 2009), as well as macroscopic particles and oxygen consumption (Bochdansky

et al., 2010). In addition, DOC can also be transported laterally from the margins where some of this dissolved carbon could be fresh (Nakatsuka et al., 2004), resulting in a relatively smaller RDOC pool. This is evidenced by the lower FDOM (a proxy for refractory DOM) in the deep NSCS and negative correlations between BCD and FDOM ($p < 0.01$; Figure 3c). Furthermore, the observed positive correlation between apparent oxygen utilization and FDOM ($P < 0.01$) indicates that refractory FDOM was produced in situ in association with particle remineralization on the time scale of this correlation (Yamashita & Tanoue, 2008).

We also estimated the contribution of DOC to the BCD of the deep ocean. The DOC decay rate was estimated as 0.06 $\mu mol\ kg^{-1}\ yr^{-1}$ in SCS intermediate water (~1,000–1,500 m), based on differences in total organic carbon (an approximation of DOC) between the SCS (42.9 $\pm$ 0.9 $\mu mol\ L^{-1}$) and the West Philippine Sea (40.3 $\pm$ 0.6 $\mu mol\ L^{-1}$; Wu et al., 2015) and ~42-yr residence time of the intermediate water (Liu & Gan, 2017). Hence, DOC contributed approximately 2–5% to the BCD at 1,000–1,500 m in the SCS, while no clear differences in total organic carbon were observed between the northern and southern basins (Dai et al., 2009). Similarly, Kim et al. (2015) estimated the DOC decay rates as 0.04, 0.08, and 0.14 $\mu mol\ kg^{-1}\ yr^{-1}$ in the East Japan Sea (>1,000 m), high-latitude North Atlantic Ocean (>1,500 m), and Mediterranean Sea (>1,000 m), respectively. Carlson et al. (2010) reported DOC decay rates ranging from 0.13 to 0.93 $\mu mol\ kg^{-1}\ yr^{-1}$ in mesopelagic and bathypelagic realms of the North Atlantic using a single-end member mixing model and multiple linear regression; this estimate contributed less than 5% to the deep BCD in the North Atlantic (Reinthaler et al., 2006).

4. Conclusions

We quantified the contributions of four main carbon sources to the dark ocean carbon demand; of these, laterally derived sinking particles were quantified for the first time. Our results showed an unbalanced carbon budget between POC exported from the euphotic zone and dark ocean BCD, but strong and perennial lateral particle transport throughout mesopelagic and bathypelagic water masses provided an organic carbon source that contributed a substantial proportion of the BCD. Additionally, a high concentration of remineralized particles resulted in high ammonium concentrations and nitrifier abundances. Consequently, dark carbon fixation sustained primarily by nitrifiers also provided a high amount of new organic carbon to heterotrophic food webs in the deep ocean. Such sequential physical-chemical-biological processes could occur globally in marginal seas, given widespread lateral transport processes that redistribute a diverse array of substances. Therefore, these processes have a significant impact on deep sea ecosystems and carbon storage.

Collectively, our measurements and estimations quantitatively support the hypothesis that laterally transported particles in the deep open ocean provide a major carbon and energy source for dark ocean ecosystems. These results further imply that lateral particle transport from margins need to be incorporated into the mechanistic understanding of the biological carbon pump to resolve the imbalance in the carbon budget of the dark ocean.

Data Availability Statement

All data in this study are available online (https://pan.xmu.edu.cn/s/ZMIBZasuTFI).

References

Alonso-González, I. J., Arístegui, J., Vilas, J. C., & Hernández-Guerra, A. (2009). Lateral POC transport and consumption in surface and deep waters of the Canary Current region: A box model study. *Global Biogeochemical Cycles*, 23, GB2007. https://doi.org/10.1029/2008GB003185

Alonso-Sáez, L., Gasol, J. M., Arístegui, J., Vilas, J. C., Vaqué, D., Duarte, C. M., & Agustí, S. (2007). Large-scale variability in surface bacterial carbon demand and growth efficiency in the subtropical northeast Atlantic Ocean. *Limnology and Oceanography*, 52(2), 533–546. https://doi.org/10.4319/lo.2007.52.2.0533

Arístegui, J., Gasol, J. M., Duarte, C. M., & Herndl, G. J. (2009). Microbial oceanography of the dark ocean's pelagic realm. *Limnology and Oceanography*, 54(5), 1501–1529. https://doi.org/10.4319/lo.2009.54.5.1501

Baltar, F., Arístegui, J., Gasol, J. M., & Herndl, G. J. (2010). Prokaryotic carbon utilization in the dark ocean: Growth efficiency, leucine-to-carbon conversion factors, and their relation. *Aquatic Microbial Ecology*, 60(3), 227–232. https://doi.org/10.3354/ame01422

Baltar, F., Arístegui, J., Gasol, J. M., Sintes, E., & Herndl, G. J. (2009). Evidence of prokaryotic metabolism on suspended particulate organic matter in the dark waters of the subtropical North Atlantic. *Limnology and Oceanography*, 54(1), 182–193. https://doi.org/10.4319/lo.2009.54.1.0182

Baltar, F., Arístegui, J., Gasol, J. M., Sintes, E., Van Aken, H. M., & Herndl, G. J. (2010). High dissolved extracellular enzymatic activity in the deep central Atlantic Ocean. *Aquatic Microbial Ecology*, 58(3), 287–302. https://doi.org/10.3354/ame01377

Baltar, F., Arístegui, J., Sintes, E., Gasol, J. M., Reinthaler, T., & Herndl, G. J. (2010). Significance of non-sinking particulate organic carbon and dark CO_2 fixation to heterotrophic carbon demand in the mesopelagic northeast Atlantic. *Geophysical Research Letters*, *37*, L09602. https://doi.org/10.1029/2010GL043105

Baltar, F., Lundin, D., Palovaara, J., Lekunberri, I., Reinthaler, T., Herndl, G. J., & Pinhassi, J. (2016). Prokaryotic responses to ammonium and organic carbon reveal alternative CO_2 fixation pathways and importance of alkaline phosphatase in the mesopelagic North Atlantic. *Frontiers in Microbiology*, *7*, 1670. https://doi.org/10.3389/fmicb.2016.01670

Biddanda, B., & Benner, R. (1997). Major contribution from mesopelagic plankton to heterotrophic metabolism in the upper ocean. *Deep Sea Research Part I: Oceanographic Research Papers*, *44*(12), 2069–2085. https://doi.org/10.1016/S0967-0637(97)00045-9

Bochdansky, A. B., van Aken, H. M., & Herndl, G. J. (2010). Role of macroscopic particles in deep-sea oxygen consumption. *Proceedings of the National Academy of Sciences*, *107*(18), 8287–8291. https://doi.org/10.1073/pnas.0913744107

Briggs, N., Dallolmo, G., & Claustre, H. (2020). Major role of particle fragmentation in regulating biological sequestration of CO_2 by the oceans. *Science*, *367*(6479), 791–793. https://doi.org/10.1126/science.aay1790

Broek, T. A. B., Bour, A. L., Ianiri, H. L., Guilderson, T. P., & McCarthy, M. D. (2019). Amino acid enantiomers in old and young dissolved organic matter: Implications for a microbial nitrogen pump. *Geochimica et Cosmochimica Acta*, *247*, 207–219. https://doi.org/10.1016/j.gca.2018.12.037

Buesseler, K. O., Antia, A. N., Chen, M., Fowler, S. W., Gardner, W. D., Gustafsson, O., et al. (2007). An assessment of the use of sediment traps for estimating upper ocean particle fluxes. *Journal of Marine Research*, *65*(3), 345–416. https://doi.org/10.1357/002224007781567621

Burd, A. B., Hansell, D. A., Steinberg, D. K., Anderson, T. R., Arístegui, J., Baltar, F., et al. (2010). Assessing the apparent imbalance between geochemical and biochemical indicators of meso- and bathypelagic biological activity: What the @$#! is wrong with present calculations of carbon budgets? *Deep Sea Research Part II: Topical Studies in Oceanography*, *57*(16), 1557–1571. https://doi.org/10.1016/j.dsr2.2010.02.022

Cai, P., Chen, W., Dai, M., Wan, Z., Wang, D., Li, Q., et al. (2008). A high-resolution study of particle export in the southern South China Sea based on ^{234}Th: ^{238}U disequilibrium. *Journal of Geophysical Research*, *113*, C04019. https://doi.org/10.1029/2007JC004268

Cai, P., Zhao, D., Wang, L., Huang, B., & Dai, M. (2015). Role of particle stock and phytoplankton community structure in regulating particulate organic carbon export in a large marginal sea. *Journal of Geophysical Research: Oceans*, *120*, 2063–2095. https://doi.org/10.1002/2014JC010432

Carlson, C. A., Hansell, D. A., Nelson, N. B., Siegel, D. A., Smethie, W. M., Khatiwala, S., et al. (2010). Dissolved organic carbon export and subsequent remineralization in the mesopelagic and bathypelagic realms of the North Atlantic basin. *Deep-sea Research Part Ii-topical Studies in Oceanography*, *57*(16), 1433–1445. https://doi.org/10.1016/j.dsr2.2010.02.013

Dai, M., Cao, Z., Guo, X., Zhai, W., Liu, Z., Yin, Z., et al. (2013). Why are some marginal seas sources of atmospheric CO_2? *Geophysical Research Letters*, *40*, 2154–2158. https://doi.org/10.1002/grl.50390

Dai, M., Meng, F., Tang, T., Kao, S. J., Lin, J., Chen, J., et al. (2009). Excess total organic carbon in the intermediate water of the South China Sea and its export to the North Pacific. *Geochemistry, Geophysics, Geosystems*, *10*, Q12002. https://doi.org/10.1029/2009GC002752

Del Giorgio, P. A., & Cole, J. J. (1998). Bacterial growth efficiency in natural aquatic systems. *Annual Review of Ecology and Systematics*, *29*(1), 503–541. https://doi.org/10.1146/annurev.ecolsys.29.1.503

Del Giorgio, P. A., Condon, R., Bouvier, T., Longnecker, K., Bouvier, C., Sherr, E., & Gasol, J. M. (2011). Coherent patterns in bacterial growth, growth efficiency, and leucine metabolism along a northeastern Pacific inshore-offshore transect. *Limnology and Oceanography*, *56*(1), 1–16. https://doi.org/10.4319/lo.2011.56.1.0001

Erb, T. J. (2011). Carboxylases in natural and synthetic microbial pathways. *Applied and Environmental Microbiology*, *77*(24), 8466–8477. https://doi.org/10.1128/AEM.05702-11

Galand, P. E., Potvin, M., Casamayor, E. O., & Lovejoy, C. (2009). Hydrography shapes bacterial biogeography of the deep Arctic Ocean. *The ISME Journal*, *4*(4), 564–576. https://doi.org/10.1038/ismej.2009.134

Gao, S., Wang, D., Yang, Y., Zhou, L., Zhao, Y., Gao, W., et al. (2015). Holocene sedimentary systems on a broad continental shelf with abundant river input: Process–product relationships. *Geological Society, London, Special Publications*, *429*(1), 223–259. https://doi.org/10.1144/sp429.4

Gasol, J. M., Alonso-Sáez, L., Vaque, D., Baltar, F., Calleja, M. L., Duarte, C. M., & Arístegui, J. (2009). Mesopelagic prokaryotic bulk and single-cell heterotrophic activity and community composition in the NW Africa–Canary Islands coastal-transition zone. *Progress in Oceanography*, *83*(1-4), 189–196. https://doi.org/10.1016/j.pocean.2009.07.014

Gaye, B., Wiesner, M. G., & Lahajnar, N. (2009). Nitrogen sources in the South China Sea, as discerned from stable nitrogen isotopic ratios in rivers, sinking particles, and sediments. *Marine Chemistry*, *114*(3–4), 72–85. https://doi.org/10.1016/j.marchem.2009.04.003

Geng, B., Xiu, P., Shu, C., Zhang, W.-Z., Chai, F., Li, S., & Wang, D. (2019). Evaluating the roles of wind- and buoyancy flux-induced mixing on phytoplankton dynamics in the northern and central South China Sea. *Journal of Geophysical Research: Oceans*, *124*, 680–702. https://doi.org/10.1029/2018JC014170

Gong, G. C., Liu, K. K., Liu, C. T., & Pai, S. C. (1992). Chemical hydrography of the South China Sea and a comparison with the West Philippine Sea. *Terrestrial Atmospheric and Oceanic Sciences*, *3*(4), 587–602. https://doi.org/10.3319/TAO.1992.3.4.587(O)

Guerrero-Feijóo, E., Sintes, E., Herndl, G. J., & Varela, M. M. (2018). High dark inorganic carbon fixation rates by specific microbial groups in the Atlantic off the Galician coast (NW Iberian margin). *Environmental Microbiology*, *20*(2), 602–611. https://doi.org/10.1111/1462-2920.13984

Herndl, G. J., & Reinthaler, T. (2013). Microbial control of the dark end of the biological pump. *Nature Geoscience*, *6*(9), 718–724. https://doi.org/10.1038/ngeo1921

Herndl, G. J., Reinthaler, T., Teira, E., van Aken, H., Veth, C., Pernthaler, A., & Pernthaler, J. (2005). Contribution of *Archaea* to total prokaryotic production in the deep Atlantic Ocean. *Applied and Environmental Microbiology*, *71*(5), 2303–2309. https://doi.org/10.1128/AEM.71.5.2303-2309.2005

Hsiao, S. S.-Y., Hsu, T.-C., Liu, J.-W., Xie, X., Zhang, Y., Lin, J., et al. (2014). Nitrification and its oxygen consumption along the turbid Chang Jiang River plume. *Biogeosciences*, *11*(7), 2083–2098. https://doi.org/10.5194/bg-11-2083-2014

Hwang, J., Eglinton, T. I., Krishfield, R. A., Manganini, S. J., & Honjo, S. (2008). Lateral organic carbon supply to the deep Canada Basin. *Geophysical Research Letters*, *35*, L11607. https://doi.org/10.1029/2008GL034271

Jiao, N., Herndl, G. J., Hansell, D. A., Benner, R., Kattner, G., Wilhelm, S. W., et al. (2010). Microbial production of recalcitrant dissolved organic matter: Long-term carbon storage in the global ocean. *Nature Reviews Microbiology*, *8*(8), 593–599. https://doi.org/10.1038/nrmicro2386

Jiao, N., Zhang, Y., Zhou, K., Li, Q., Dai, M., Liu, J., et al. (2014). Revisiting the CO₂ "source" problem in upwelling areas—A comparative study on eddy upwellings in the South China Sea. *Biogeosciences*, *11*(9), 2465–2475. https://doi.org/10.5194/bg-11-2465-2014

Kao, S. J., Dai, M., Selvaraj, K., Zhai, W., Cai, P., Chen, S. N., et al. (2010). Cyclone-driven deep sea injection of freshwater and heat by hyperpycnal flow in the subtropics. *Geophysical Research Letters*, *37*, L21702. https://doi.org/10.1029/2010GL044893

Kao, S.-J., Yang, J.-Y. T., Liu, K.-K., Dai, M., Chou, W.-C., Lin, H.-L., & Ren, H. (2012). Isotope constraints on particulate nitrogen source and dynamics in the upper water column of the oligotrophic South China Sea. *Global Biogeochemical Cycles*, *26*, GB2033. https://doi.org/10.1029/2011GB004091

Kim, T.-H., Kim, G., Lee, S.-A., & Dittmar, T. (2015). Extraordinary slow degradation of dissolved organic carbon (DOC) in a cold marginal sea. *Scientific Reports*, *5*(1), 13,808–13,808. https://doi.org/10.1038/srep13808

Kitzinger, K., Padilla, C. C., Marchant, H. K., Hach, P. F., Herbold, C. W., Kidane, A. T., et al. (2018). Cyanate and urea are substrates for nitrification by Thaumarchaeota in the marine environment. *Nature Microbiology*, *4*(2), 234–243. https://doi.org/10.1038/s41564-018-0316-2

Lahajnar, N., Wiesner, M. G., & Gaye, B. (2007). Fluxes of amino acids and hexosamines to the deep South China Sea. *Deep Sea Research Part I: Oceanographic Research Papers*, *54*(12), 2120–2144. https://doi.org/10.1016/j.dsr.2007.08.009

Liu, C.-T., & Liu, R.-J. (1988). The deep current in the Bashi Channel. *Acta Oceanographica. Taiwan*, *20*, 107–116.

Liu, Z., & Gan, J. (2017). Three-dimensional pathways of water masses in the South China Sea: A modeling study. *Journal of Geophysical Research: Oceans*, *122*, 6039–6054. https://doi.org/10.1002/2016JC012511

Martin, J. H., Knauer, G. A., Karl, D. M., & Broenkow, W. W. (1987). VERTEX: Carbon cycling in the northeast Pacific. *Deep-Sea Research*, *34*(2), 267–285. https://doi.org/10.1016/0198-0149(87)90086-0

Mazuecos, I. P., Arístegui, J., Vázquez-Domínguez, E., Ortega-Retuerta, E., Gasol, J. M., & Reche, I. (2015). Temperature control of microbial respiration and growth efficiency in the mesopelagic zone of the South Atlantic and Indian Oceans. *Deep Sea Research Part I: Oceanographic Research Papers*, *95*, 131–138. https://doi.org/10.1016/j.dsr.2014.10.014

Morán, X. A., Fernández, E., & Pérez, V. (2004). Size-fractionated primary production, bacterial production and net community production in subtropical and tropical domains of the oligotrophic NE Atlantic in autumn. *Marine Ecology Progress Series*, *274*, 17–29. https://doi.org/10.3354/meps274017

Motegi, C., Nagata, T., Miki, T., Weinbauer, M. G., Legendre, L., & Rassoulzadegand, F. (2009). Viral control of bacterial growth efficiency in marine pelagic environments. *Limnology and Oceanography*, *54*(6), 1901–1910. https://doi.org/10.4319/lo.2009.54.6.1901

Nagata, T., Fukuda, H., Fukuda, R., & Koike, I. (2000). Bacterioplankton distribution and production in deep Pacific waters: Large-scale geographic variations and possible coupling with sinking particle fluxes. *Limnology and Oceanography*, *45*(2), 426–435. https://doi.org/10.4319/lo.2000.45.2.0426

Nakatsuka, T., Toda, M., Kawamura, K., & Wakatsuchi, M. (2004). Dissolved and particulate organic carbon in the Sea of Okhotsk: Transport from continental shelf to ocean interior. *Journal of Geophysical Research*, *109*, C09S14. https://doi.org/10.1029/2003JC001909

Qu, T., Girton, J. B., & Whitehead, J. A. (2006). Deepwater overflow through Luzon Strait. *Journal of Geophysical Research*, *111*, C01002. https://doi.org/10.1029/2005JC003139

Ran, L., Chen, J., Wiesner, M. G., Ling, Z., Lahajnar, N., Yang, Z., et al. (2015). Variability in the abundance and species composition of diatoms in sinking particles in the northern South China Sea: Results from time-series moored sediment traps. *Deep-sea Research Part II-Topical Studies in Oceanography*, *122*, 15–24. https://doi.org/10.1016/j.dsr2.2015.07.004

Reinthaler, T., van Aken, H., Veth, C., Arístegui, J., Robinson, C., Williams, P. J. B., et al. (2006). Prokaryotic respiration and production in the meso- and bathypelagic realm of the eastern and western North Atlantic basin. *Limnology and Oceanography*, *51*(3), 1262–1273. https://doi.org/10.4319/lo.2006.51.3.1262

Schroeder, A., Wiesner, M. G., & Liu, Z. (2015). Fluxes of clay minerals in the South China Sea. *Earth and Planetary Science Letters*, *430*, 30–42. https://doi.org/10.1016/j.epsl.2015.08.001

Sherr, E. B., Sherr, B. F., & Sigmon, C. T. (1999). Activity of marine bacteria under incubated and in situ conditions. *Aquatic Microbial Ecology*, *20*(3), 213–223. https://doi.org/10.3354/ame020213

Shih, Y.-Y., Lin, H.-H., Li, D., Hsieh, H.-H., Hung, C.-C., & Chen, C.-T. A. (2019). Elevated carbon flux in deep waters of the South China Sea. *Scientific Reports*, *9*(1), 1496–1498. https://doi.org/10.1038/s41598-018-37726-w

Spall, M. A., & Pedlosky, J. (2018). Shelf–open ocean exchange forced by wind jets. *Journal of Physical Oceanography*, *48*(1), 163–174. https://doi.org/10.1175/jpo-d-17-0161.1

Steinberg, D. K., Van Mooy, B. A. S., Buesseler, K. O., Boyd, P. W., Kobari, T., & David, M. K. (2008). Bacterial vs. zooplankton control of sinking particle flux in the ocean's twilight zone. *Limnology and Oceanography*, *53*(4), 1327–1338. https://doi.org/10.4319/lo.2008.53.4.1327

Suess, E. (1980). Particulate organic carbon flux in the oceans—Surface productivity and oxygen utilization. *Nature*, *288*(5788), 260–263. https://doi.org/10.1038/288260a0

Swan, B. K., Martinez-Garcia, M., Preston, C. M., Sczyrba, A., Woyke, T., Lamy, D., et al. (2011). Potential for chemolithoautotrophy among ubiquitous bacteria lineages in the dark ocean. *Science*, *333*(6047), 1296–1300. https://doi.org/10.1126/science.1203690

Tan, S., Zhang, J., Li, H., Sun, L., Wu, Z., Wiesner, M. G., et al. (2020). Deep ocean particle flux in the northern South China Sea: Variability on intra-seasonal to seasonal timescales. *Frontiers in Earth Science*, *8*, 74. https://doi.org/10.3389/feart.2020.00074

Teira, E., Lebaron, P., van Aken, H., & Herndl, G. J. (2006). Distribution and activity of bacteria and archaea in the deep water masses of the North Atlantic. *Limnology and Oceanography*, *51*(5), 2131–2144. https://doi.org/10.4319/lo.2006.51.5.2131

Uchimiya, M., Fukuda, H., Wakita, M., Kitamura, M., Kawakami, H., Honda, M. C., et al. (2018). Balancing organic carbon supply and consumption in the ocean's interior: Evidence from repeated biogeochemical observations conducted in the subarctic and subtropical western North Pacific. *Limnology and Oceanography*, *63*(5), 2015–2027. https://doi.org/10.1002/lno.10821

Uchimiya, M., Ogawa, H., & Nagata, T. (2015). Effects of temperature elevation and glucose addition on prokaryotic production and respiration in the mesopelagic layer of the western North Pacific. *Journal of Oceanography*, *72*(3), 419–426. https://doi.org/10.1007/s10872-015-0294-4

Vázquez-Domínguez, E., Duarte, C. M., Agustí, S., Jürgens, K., Vaqué, D., & Gasol, J. M. (2008). Microbial plankton abundance and heterotrophic activity across the Central Atlantic Ocean. *Progress in Oceanography*, *79*(1), 83–94. https://doi.org/10.1016/j.pocean.2008.08.002

Wang, D., Wang, Q., Cai, S., Shang, X., Peng, S., Shu, Y., et al. (2019). Advances in research of the mid-deep South China Sea circulation. *Science China Earth Sciences*, *62*(12), 1992–2004. https://doi.org/10.1007/s11430-019-9546-3

Wang, G., Su, J., & Chu, P. C. (2003). Mesoscale eddies in the South China Sea observed with altimeter data. *Geophysical Research Letters*, *30*(21), 2121. https://doi.org/10.1029/2003GL018532

Wei, C.-L., Chia, C.-Y., Chou, W.-C., & Lee, W.-H. (2017). Sinking fluxes of ^{210}Pb and ^{210}Po in the deep basin of the northern South China Sea. *Journal of Environmental Radioactivity*, *174*, 45–53. https://doi.org/10.1016/j.jenvrad.2016.05.026

Wu, K., Dai, M., Chen, J., Meng, F., Li, X., Liu, Z., et al. (2015). Dissolved organic carbon in the South China Sea and its exchange with the Western Pacific Ocean. *Deep Sea Research Part II: Topical Studies in Oceanography*, *122*, 41–51. https://doi.org/10.1016/j.dsr2.2015.06.013

Wuchter, C., Abbas, B., Coolen, M. J. L., Herfort, L., van Bleijswijk, J., Timmers, P., et al. (2006). Archaeal nitrification in the ocean. *Proceedings of the National Academy of Sciences of the United States of America*, *103*(33), 12,317–12,322. https://doi.org/10.1073/pnas.0600756103

Xiu, P., Chai, F., Shi, L., Xue, H., & Chao, Y. (2010). A census of eddy activities in the South China Sea during 1993–2007. *Journal of Geophysical Research*, *115*, C03012. https://doi.org/10.1029/2009JC005657

Yamashita, Y., & Tanoue, E. (2008). Production of bio-refractory fluorescent dissolved organic matter in the ocean interior. *Nature Geoscience*, *1*(9), 579–582. https://doi.org/10.1038/ngeo279

Yang, J.-Y. T., Kao, S.-J., Dai, M., Yan, X., & Lin, H.-L. (2017). Examining N cycling in the northern South China Sea from N isotopic signals in nitrate and particulate phases. *Journal of Geophysical Research: Biogeosciences*, *122*, 2118–2136. https://doi.org/10.1002/2016JG003618

Yang, W., Chen, M., Zheng, M., He, Z., Zhang, X., Qiu, Y., et al. (2015). Influence of a decaying cyclonic eddy on biogenic silica and particulate organic carbon in the Tropical South China Sea based on ^{234}Th-^{238}U disequilibrium. *PLoS ONE*, *10*(8), e0136948. https://doi.org/10.1371/journal.pone.0136948

Zhang, J., Li, H., Xuan, J., Wu, Z., Yang, Z., Wiesner, M. G., & Chen, J. (2019). Enhancement of mesopelagic sinking particle fluxes due to upwelling, aerosol deposition, and monsoonal influences in the northwestern South China Sea. *Journal of Geophysical Research: Oceans*, *124*, 99–112. https://doi.org/10.1029/2018JC014704

Zhang, Y., Liu, Z., Zhao, Y., Wang, W., Li, J., & Xu, J. (2014). Mesoscale eddies transport deep-sea sediments. *Scientific Reports*, *4*(1), 5937. https://doi.org/10.1038/srep05937

Zhang, Y., Qin, W., Hou, L., Zakem, E. J., Wan, X., Zhao, Z., et al. (2020). Nitrifier adaptation to low energy flux controls inventory of reduced nitrogen in the dark ocean. *Proceedings of the National Academy of Sciences*, *117*(9), 4823–4830. https://doi.org/10.1073/pnas.1912367117

Zhang, Y., Zhao, Z., Dai, M., Jiao, N., & Herndl, G. J. (2014). Drivers shaping the diversity and biogeography of total and active bacterial communities in the South China Sea. *Molecular Ecology*, *23*(9), 2260–2274. https://doi.org/10.1111/mec.12739

Zhou, K., Dai, M., Kao, S.-J., Wang, L., Xiu, P., Chai, F., et al. (2013). Apparent enhancement of ^{234}Th-based particle export associated with anticyclonic eddies. *Earth and Planetary Science Letters*, *381*, 198–209. https://doi.org/10.1016/j.epsl.2013.07.039

Zhu, Y. (2015). *Distribution and dynamics of ammonium in the South China Sea (Master's thesis)*. Xiamen, China: Xiamen University.

Zubkov, M. V., Sleigh, M. A., Burkill, P. H., & Leakey, R. J. G. (2000). Bacterial growth and grazing loss in contrasting areas of North and South Atlantic. *Journal of Plankton Research*, *22*(4), 685–711. https://doi.org/10.1093/plankt/22.4.685